Supplement of Atmos. Chem. Phys., 23, 13597–13611, 2023
https://doi.org/10.5194/acp-23-13597-2023-supplement

Supplement of

Mixing state and effective density of aerosol particles during the Beijing 2022 Olympic Winter Games

Aodong Du et al.

Correspondence to: Yele Sun (sunyele@mail.iap.ac.cn)

1.1 Instrument

1.1.1 SPAMS

A high-resolution single particle aerosol mass spectrometer (HR-SPAMS, Hexin Analytical Instrument Co., Ltd., China) was used to determine the size distribution and chemical composition of individual particles in real time. Briefly, aerosol particles are drawn into the aerodynamic lens through a 0.1 mm critical flow orifice. The accelerated particle beam passes through two consecutive laser beams (Nd: YAG laser, 532 nm) successively and obtains its flight speed as well as vacuum aerodynamic diameter (D_{va}) accordingly. Subsequently, particles with the specific velocity will precisely trigger the pulsed laser (Nd: YAG laser, 266 nm) and the ion fragments produced by ionization are recorded by a time-of-flight mass spectrometer. More detailed description of the traditional SPAMS is available in Li et al. (2011). HR-SPAMS has a higher mass resolution and transport efficiency of particles compared to the traditional SPAMS (Zhu et al., 2020).

1.1.2 DMA

A differential mobility analyzer (DMA, model 3085A, TSI Inc., USA) was used to select a particle population with a narrow distribution of mobility diameters (D_m). Highly monodisperse particles with a range of specific D_m are output by controlling the voltage in the DMA, while other particles are discarded (Decarlo et al., 2004; Cotterell et al., 2020; Fuchs et al., 1965).

1.1.3 AAC

An aerodynamic aerosol classifier (AAC, Cambustion Ltd., UK) was deployed to select monodisperse particles classified by their aerodynamic diameters (D_a). Only particles in the narrower D_a range will follow the correct trajectory and flow through the AAC classifier influenced by both centrifugal and dragging forces. Details on the principles of AAC can be found in Tavakoli and Olfert (2013).

1.2 Calculation of effective density

So far, three definitions of effective density (ρ_{eff}) have been introduced in atmospheric science research (Decarlo et al., 2004; Hand and Kreidenweis, 2002), one of which is defined as the ratio of vacuum aerodynamic diameter to mobility diameter.

$$\rho_{eff} = \frac{D_{va}}{D_m} \rho_0 \tag{1}$$

It can be used to calculate the ρ_{eff} of particles captured by the DMA-SPAMS tandem system. Where ρ_0 is the standard density (1.0 g cm^{-3}). It is important to note that D_{va} measurements can easily resolve particles with identical mobility but with different charges. Although the majority of size-selected particles exiting the DMA contain +1 electrostatic charge, there is still a small fraction of particles containing more than +1 charge. Based on this, particles with different charge numbers can be distinguished by different D_{va} according to the following equation:

$$\frac{D_p}{C_c} = \frac{2neVL}{3\mu q_{sh} \ln\left(\frac{r_2}{r_1}\right)} \tag{2}$$

where the DMA set voltage (V) and rod length (L), gas viscosity (μ), sheath flow (q_{sh}), inner and outer radius (r_1 and r_2) of the DMA annular space are known. As described by Knutson and Whitby (1976), C_c is the Cunningham slip factor evaluated at a certain physical diameter (D_p) and n is the number of charges carried by the particles. D_p will be equal to D_m when the number of charges on the particle is equal to one while it will be greater than D_m for charges greater than one (Spencer et al., 2007).

Another approach to define the ρ_{eff} that can be adopted in the AAC-SPAMS tandem system is based on the ratio of particle density (ρ_p) and the particle dynamic shape factor (χ_γ) as follows:

$$\rho_{eff} = \frac{\rho_p}{\chi_\gamma} \tag{3}$$

Combined with the calculation of D_{va} proposed by Jimenez (2003) (Eq. (4)), ρ_{eff} can be obtained as follows:

$$D_{va} = \frac{\rho_p D_{ve}}{\rho_0 \chi_\gamma} \tag{4}$$

$$\rho_{eff} = \frac{D_{va}}{D_{ve}\rho_0} \tag{5}$$

where D_{ve} represents the volume equivalent diameter. The method of deriving the particle effective density with the support of D_{ve} and D_{va} has been verified in detail in previous studies (Peng et al., 2021; Su et al., 2021). The relationship between the D_a, D_{va} and D_{ve} can be stated by the following equation:

$$D_a = D_{ve}\sqrt{\frac{\rho_p C_c(D_{ve})}{\chi_t \rho_0 C_c(D_a)}} \tag{6}$$

where χ_t represents the aerosol dynamic shape factor in the transition regime. Considering the approximation between χ_t and χ_γ, the D_{ve} can be calculated by combining Eqs. (5) and (6) as follows:

$$C_c(D_a)\frac{D_a^2}{D_{va}} = D_{ve} C_c(D_{ve}) \tag{7}$$

Moreover, it's necessary to dry the ambient aerosols before sampling, otherwise the evaporation of water from the particles in the aerodynamic lens has the potential to cause measurement errors in D_{va} and ρ_{eff} (Zelenyuk et al., 2006).

Table S1: Summary of the sampling periods, the number of hit particles, the average mass concentrations of NR-PM$_1$ and eBC, and the average absorption Ångström exponent (AAE) for different particle size-selection periods.

	Duration	MASS	NR-PM$_1$ (μg m^{-3})	eBC (μg m^{-3})	AAE
D_m=200nm	1.21-2.2	320093	23.93	2.12	1.40
D_m=250nm	2.2-2.5	37498	2.46	0.36	1.49
D_m=300nm	2.5-2.8	32909	2.85	0.46	1.48
D_m=150nm	2.8-2.10	46651	10.69	1.80	1.48
D_a=300nm	2.10-3.1	322415	8.70	1.16	1.37

Table S2: Description of the different particle classes and summary of the characteristic peaks.

Description of different classes	Characteristic peaks
pure-EC	$C_n^{\pm}$, n = 1, 2, 3…
	(Xie et al., 2020; Liu et al., 2019)
EC internally mixed with nitrate and sulfate (EC-NS)	46[NO_2]$^-$, 62[NO_3]$^-$ and $C_n^{\pm}$
	(Chen et al., 2020; Dall'osto and Harrison, 2012)
K rich EC, internally mixed with nitrate (KEC-N)	39[K]$^+$, 46[NO_2]$^-$, 62[NO_3]$^-$ and $C_n^{\pm}$
	(Li et al., 2014; Healy et al., 2013)
K and Na rich EC, internally mixed with nitrate (KNaEC-N)	39[K]$^+$, 23[Na]$^+$, 46[NO_2]$^-$, 62[NO_3]$^-$ and $C_n^{\pm}$
	(Li et al., 2018; Toner et al., 2008)
ECOC internally mixed with nitrate and sulfate (ECOC-NS)	46[NO_2]$^-$, 62[NO_3]$^-$, 97[HSO_4]$^-$, $C_n^{\pm}$ and OC peaks (including 27[C_2H_3]$^+$, 37[C_3H]$^+$, 43[C_2H_3O]$^+$, 50[C_4H_2]$^+$, 51[C_4H_3]$^+$…)
	(Sun et al., 2022a; Sun et al., 2022b; Xie et al., 2020)
K rich ECOC, internally mixed with nitrate and sulfate (KECOC-NS)	39[K]$^+$, 46[NO_2]$^-$, 62[NO_3]$^-$, 97[HSO_4]$^-$, $C_n^{\pm}$ and OC peaks
	(Moffet et al., 2008; Zhang et al., 2008)
K rich ECOC, internally mixed with cyanide (KECOC-CN)	39[K]$^+$, 26[CN]$^-$, 42[CNO]$^-$, $C_n^{\pm}$ and OC peaks
	(Lu et al., 2017; Pratt et al., 2009)
K and Na rich ECOC, internally mixed with nitrate and sulfate (KNaECOC-NS)	39[K]$^+$, 23[Na]$^+$, 46[NO_2]$^-$, 62[NO_3]$^-$, 97[HSO_4]$^-$, $C_n^{\pm}$ and OC peaks
	(Li et al., 2014; Gard et al., 1998)
K rich ECOC, internally mixed with nitrate, sulfate and ammonium (KAECOC-NS)	39[K]$^+$, 18[NH_4]$^+$, 46[NO_2]$^-$, 62[NO_3]$^-$, 97[HSO_4]$^-$, $C_n^{\pm}$ and OC peaks
	(Zhong et al., 2022; Gross et al., 2000)
K rich OC, internally mixed with nitrate (KOC-N)	39[K]$^+$, 46[NO_2]$^-$, 62[NO_3]$^-$ and OC peaks
	(Bi et al., 2011)
K rich OC, internally mixed with nitrate and sulfate (KOC-NS)	39[K]$^+$, 46[NO_2]$^-$, 62[NO_3]$^-$, 97[HSO_4]$^-$ and OC peaks
	(Spencer et al., 2007; Bi et al., 2011)

K rich organic amine, internally mixed with nitrate and sulfate (K-Amine-NS)	39[K]$^+$, 58[C_3H_8N]$^+$, 59[C_3H_9N]$^+$, 46[NO_2]$^-$, 62[NO_3]$^-$, 97[HSO_4]$^-$ and OC peaks
	(Chen et al., 2019; Angelino et al., 2001; Cheng et al., 2018)
K rich particles from biomass combustion (Biomass-K)	39[K]$^+$, 45[CHO_2]$^-$, 59[$C_2H_3O_2$]$^-$, 71[C_3H_3O]$^-$ and 73[$C_3H_5O_2$]$^-$
	(Hatch et al., 2014; Silva et al., 1999; Guazzotti et al., 2003)
High-molecular-weight organic matter (HOM)	152[$C_{12}H_8$]$^+$, 165[$C_{13}H_9$]$^+$, 178[$C_{14}H_{10}$]$^+$, 189[$C_{15}H_9$]$^+$…
	(Zhang et al., 2022; Drewnick et al., 2008; Toner et al., 2006)
K rich particles, internally mixed with nitrate (K-N)	39[K]$^+$, 46[NO_2]$^-$ and 62[NO_3]$^-$
	(Dall'osto et al., 2008)
K and Na rich particles, internally mixed with nitrate (KNa-N)	39[K]$^+$, 23[Na]$^+$, 46[NO_2]$^-$ and 62[NO_3]$^-$
	(Guo et al., 2010)
Fe rich particles (rich-Fe)	56[Fe]$^+$ and 54[Fe]$^+$
	(Wang et al., 2016; Zhang et al., 2014; Furutani et al., 2011)

Table S3: A summary of particle types and number of particles captured per day for the OWG and nOWG periods.

Classification of particles		OWG	nOWG	OWG (per day)	nOWG (per day)
Total-EC	pure-EC	1155	2162	68	94
	EC-NS	8845	39761	520	1729
	KEC-N	4947	21303	291	926
	KNaEC-N	7039	14037	414	610
Total-ECOC	ECOC-NS	50382	58108	2964	2526
	KECOC-CN	3602	4891	212	213
	KECOC-NS	60631	109959	3567	4781
	KNaECOC-NS	13725	22096	807	961
	KAECOC-NS	662	23314	39	1014
Total-OC	KOC-N	13078	25298	769	1100
	KOC-NS	12242	18998	720	826
	K-Amine-NS	1219	6446	72	280
Total-IA	K-N	11561	24385	680	1060
	KNa-N	6215	9693	366	421
Biomass-K		41627	54526	2449	2371
HOM		16610	24388	977	1060
Metals	rich-Fe	1474	14088	87	613
	other	3542	7245	208	315

Table S4: Correlation analysis between the number concentration of each particle type and the mass concentration of the chemical components measured by HR-ToF-AMS. Higher similarities

are marked with *.

	FFBBOA	COA	OOA1	OOA2	aqOOA	Org	SO_4	NO_3	NH_4	Chl
pure-EC	0.25	0.47	0.20	-0.03	0.04	0.23	0.01	0.14	0.11	0.24
EC-NS	0.15	0.17	0.75*	0.81*	0.71*	0.76	0.74	0.82	0.82	0.56
KEC-N	0.32	0.27	0.85*	0.79*	0.77*	0.85	0.80	0.87	0.88	0.80*
KNaEC-N	0.74*	0.56	0.69	0.25	0.41	0.67	0.35	0.54	0.50	0.74*
ECOC-NS	0.44	0.14	0.29	0.14	0.27	0.32	0.36	0.25	0.29	0.36
KECOC-NS	0.78*	0.60	0.63	0.31	0.48	0.69	0.45	0.52	0.51	0.67
KECOC-CN	0.27	0.14	-0.09	-0.08	0.13	0.05	0.08	-0.04	0	0.18
KNaECOC-NS	0.80*	0.55	0.70*	0.23	0.41	0.67	0.40	0.51	0.49	0.70*
KAECOC-NS	0.27	0.17	0.77*	0.76*	0.79*	0.79	0.85	0.80	0.84	0.67
KOC-N	0.70*	0.67	0.33	0.06	0.22	0.45	0.12	0.24	0.21	0.45
KOC-NS	0.69	0.72*	0.66	0.31	0.49	0.73	0.47	0.55	0.54	0.71*
K-Amine-NS	0.01	0.03	0.55	0.83*	0.66	0.63	0.69	0.71	0.73	0.45
Biomass-K	0.55	0.73*	0.26	0.12	0.03	0.32	-0.04	0.09	0.06	0.32
HOM	0.47	0.03	-0.07	-0.09	0.11	0.05	0.08	-0.04	-0.01	0.19
K-N	0.62	0.51	0.82*	0.61	0.74*	0.89	0.75	0.79	0.81	0.86*
KNa-N	0.63	0.52	0.54	0.22	0.40	0.58	0.32	0.42	0.40	0.58

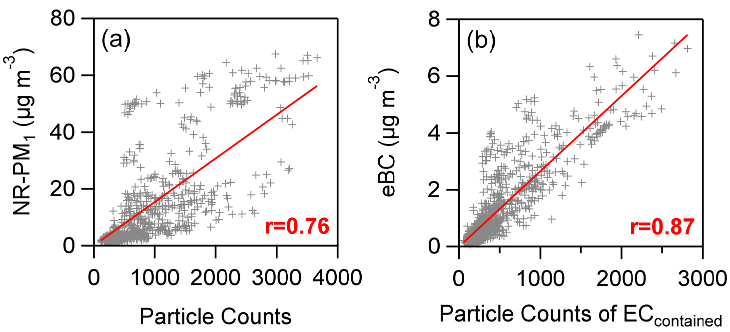

Figure S1: Scatter plots of the (a) total particle counts and (b) EC-containing particle counts captured by SPAMS versus the mass concentrations of NR-PM$_1$ and eBC measured by AMS and AE33.

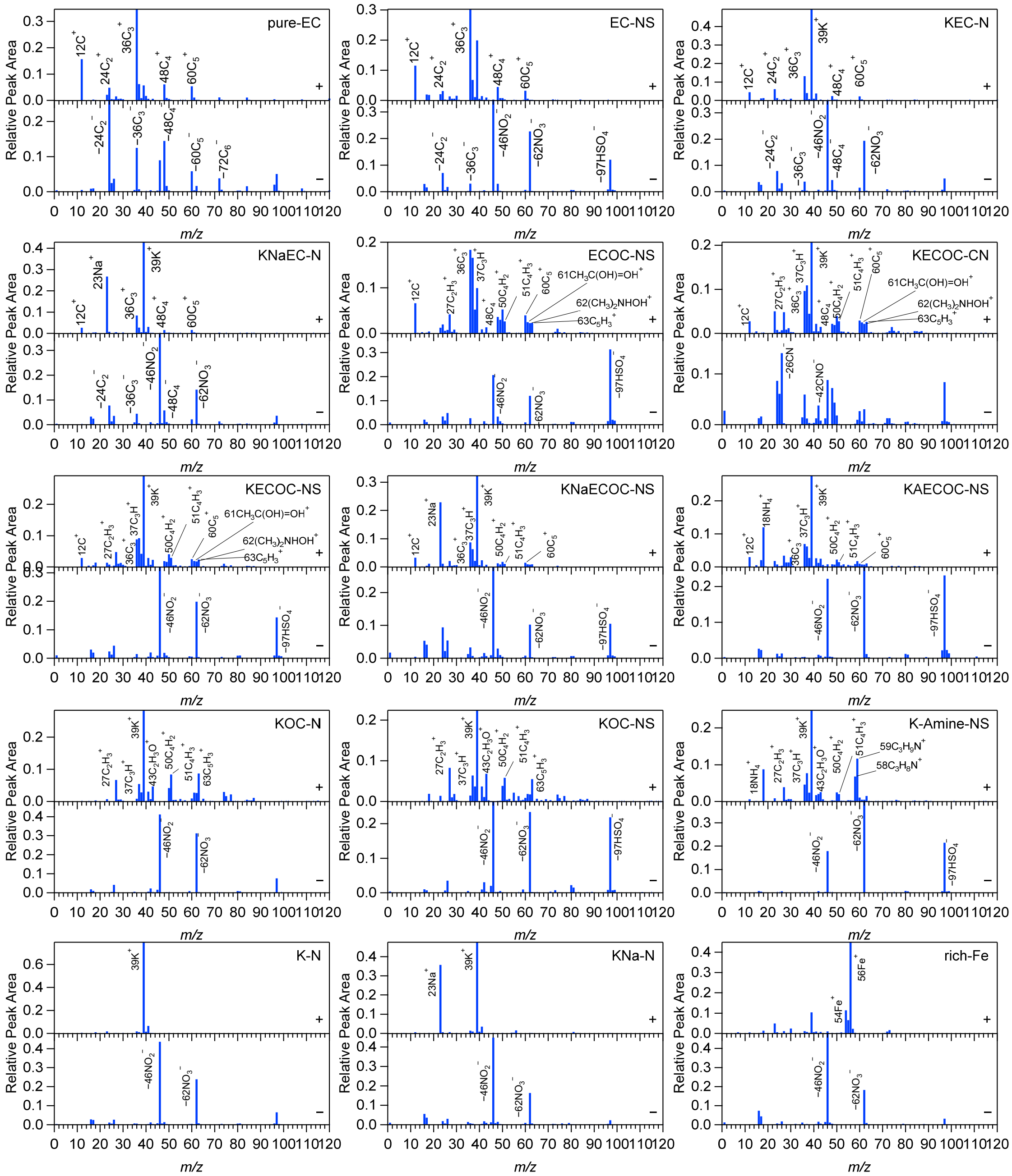

Figure S2: Average mass spectra of each subclass of particles.

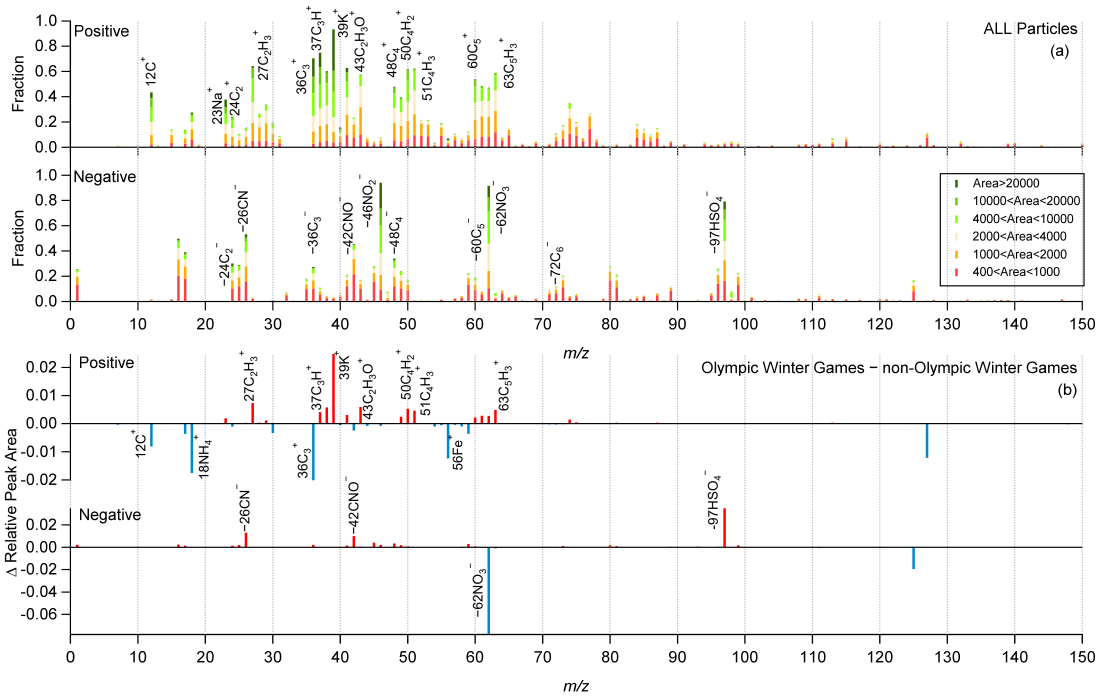

Figure S3: The (a) digital mass spectra of all particles throughout the campaign (where the ion heights in the spectrum represent their proportions and the colors represent the range of peak area intensities), and (b) the differences in the average mass spectra of particles during the Olympic Winter Games and non- Olympic Winter Games periods.

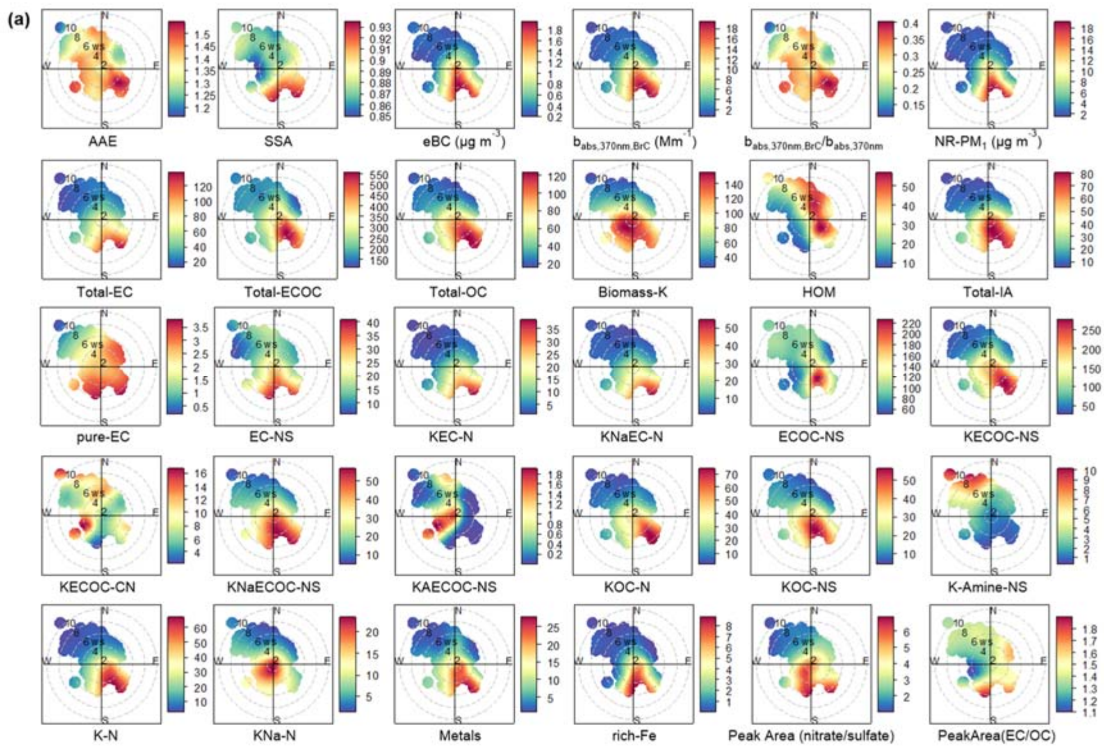

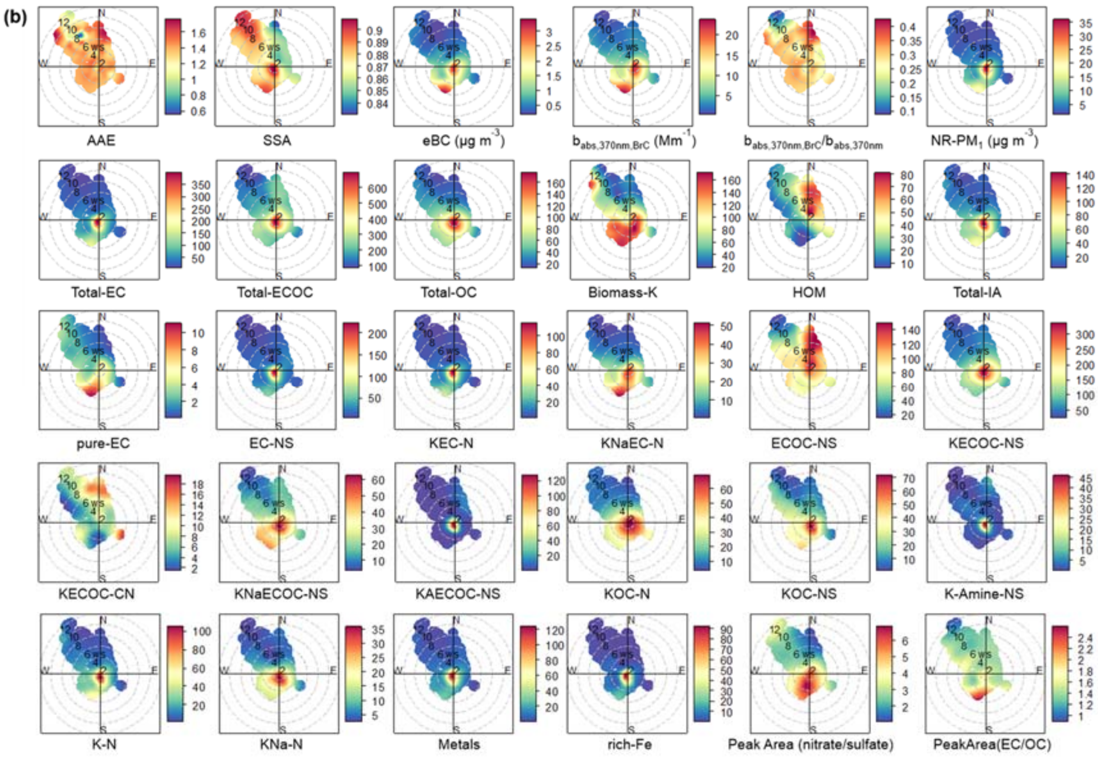

Figure S4: Bivariate polar plots of different types of particles and other parameters during (a) Olympic Winter Games and (b) non-Olympic Winter Games. The color bars in the bivariate polar plots for the seven major and fifteen minor classes of particles (Table 1), eBC and NR-PM1, and $b_{abs,370nm,BrC}$ correspond to the particle counts, mass concentrations, and absorption coefficients, respectively.

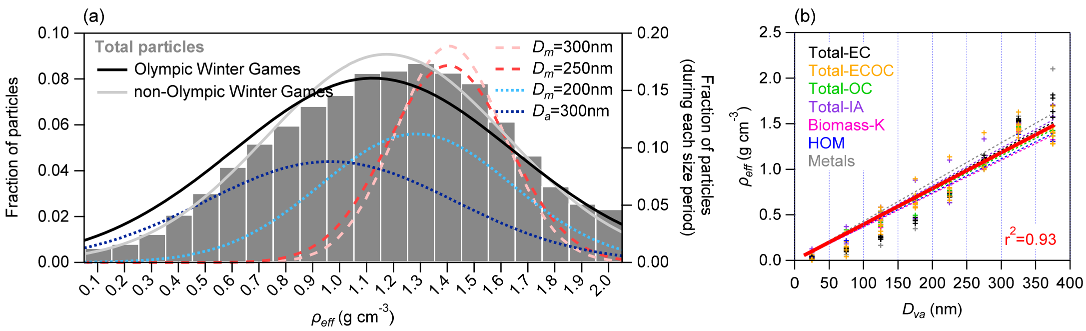

Figure S5: Distributions of effective density of particles for different periods (a). The left y–axis is applied to the column diagram as well as OWG and now periods, and the right y–axis is applied to the Gaussian fitting curves for each size-resolution period. And variations of effective density as a function of D_{va} (b).

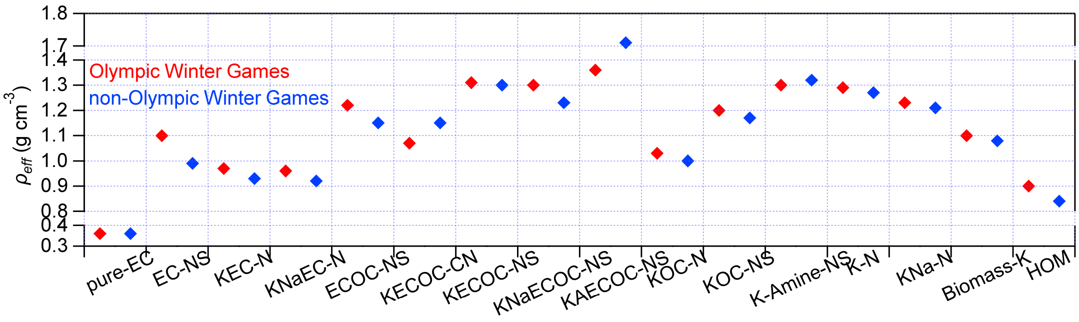

Figure S6: Average effective density of different classes of particles during the OWG and nOWG periods.

References

Angelino, S., Suess, D. T., and Prather, K. A.: Formation of Aerosol Particles from Reactions of Secondary and Tertiary Alkylamines: Characterization by Aerosol Time-of-Flight Mass Spectrometry, Environ. Sci. Technol., 35, 3130-3138, doi:10.1021/es0015444 2001.

Bi, X., Zhang, G., Li, L., Wang, X., Li, M., Sheng, G., Fu, J., and Zhou, Z.: Mixing state of biomass burning particles by single particle aerosol mass spectrometer in the urban area of PRD, China, Atmos. Environ., 45, 3447-3453, doi:10.1016/j.atmosenv.2011.03.034, 2011.

Chen, Y., Tian, M., Huang, R.-J., Shi, G., Wang, H., Peng, C., Cao, J., Wang, Q., Zhang, S., Guo, D., Zhang, L., and Yang, F.: Characterization of urban amine-containing particles in southwestern China: seasonal variation, source, and processing, Atmos. Chem. Phys., 19, 3245-3255, doi:10.5194/acp-19-3245-2019, 2019.

Chen, Y., Cai, J., Wang, Z., Peng, C., Yao, X., Tian, M., Han, Y., Shi, G., Shi, Z., Liu, Y., Yang, X., Zheng, M., Zhu, T., He, K., Zhang, Q., and Yang, F.: Simultaneous measurements of urban and rural particles in Beijing – Part 1: Chemical composition and mixing state, Atmos. Chem. Phys., 20, 9231-9247, doi:10.5194/acp-20-9231-2020, 2020.

Cheng, C., Huang, Z., Chan, C. K., Chu, Y., Li, M., Zhang, T., Ou, Y., Chen, D., Cheng, P., Li, L., Gao, W., Huang, Z., Huang, B., Fu, Z., and Zhou, Z.: Characteristics and mixing state of amine-containing particles at a rural site in the Pearl River Delta, China, Atmos. Chem. Phys., 18, 9147-9159, doi:10.5194/acp-18-9147-2018, 2018.

Cotterell, M. I., Szpek, K., Haywood, J. M., and Langridge, J. M.: Sensitivity and accuracy of refractive index retrievals from measured extinction and absorption cross sections for mobility-selected internally mixed light absorbing aerosols, Aerosol Sci. Tech., 54, 1034-1057, doi:10.1080/02786826.2020.1757034, 2020.

Dall'Osto, M. and Harrison, R. M.: Urban organic aerosols measured by single particle mass spectrometry in the megacity of London, Atmos. Chem. Phys., 12, 4127-4142, doi:10.5194/acp-12-4127-2012, 2012.

Dall'Osto, M., Booth, M. J., Smith, W., Fisher, R., and Harrison, R. M.: A Study of the Size Distributions and the Chemical Characterization of Airborne Particles in the Vicinity of a Large Integrated Steelworks, Aerosol Sci. Tech., 42, 981-991, doi:10.1080/02786820802339587, 2008.

DeCarlo, P. F., Slowik, J. G., Worsnop, D. R., Davidovits, P., and Jimenez, J. L.: Particle Morphology and Density Characterization by Combined Mobility and Aerodynamic Diameter Measurements. Part 1: Theory, Aerosol Sci. Tech., 38, 1185-1205, doi:10.1080/027868290903907, 2004.

Drewnick, F., Dall'Osto, M., and Harrison, R.: Characterization of aerosol particles from grass mowing by joint deployment of ToF-AMS and ATOFMS instruments, Atmos. Environ., 42, 3006-3017, doi:10.1016/j.atmosenv.2007.12.047, 2008.

Fuchs, N. A., Daisley, R. E., Fuchs, M., Davies, C. N., and Straumanis, M. E.: The Mechanics of Aerosols, Phys. Today, 18, doi:10.1063/1.3047354, 1965.

Furutani, H., Jung, J., Miura, K., Takami, A., Kato, S., Kajii, Y., and Uematsu, M.: Single-particle chemical characterization and source apportionment of iron-containing atmospheric aerosols in Asian outflow, J. Geophys. Res., 116, D18204, doi:10.1029/2011jd015867, 2011.

Gard, E. E., Kleeman, M. J., Gross, D. S., Hughes, L. S., Allen, J. O., Morrical, B. D., Fergenson, D. P., Dienes, T., Galli, M. E., Johnson, R. J., Cass, G. R., and Prather, K. A.: Direct observation of heterogeneous chemistry in the atmosphere, Science, 279, 1184-1187, doi:10.1126/science.279.5354.1184, 1998.

Gross, D. S., Galli, M. E., Silva, P. J., and Prather, K. A.: Relative sensitivity factors for alkali metal and ammonium cations in single-particle aerosol time-of-flight mass spectra, Anal Chem, 72, 416-422, doi:10.1021/ac990434g, 2000.

Guazzotti, S. A., Suess, D. T., Coffee, K. R., Quinn, P. K., Bates, T. S., Wisthaler, A., Hansel, A., Ball, W. P., Dickerson, R. R., Neususs, C., Crutzen, P. J., and Prather, K. A.: Characterization of carbonaceous aerosols outflow from India and Arabia: Biomass/biofuel burning and fossil fuel combustion, J. Geophys. Res., 108, 4485, doi:10.1029/2002jd003277, 2003.

Guo, S., Hu, M., Wang, Z., Slanina, J., and Zhao, Y.: Size-resolved aerosol water-soluble ionic compositions in the summer of Beijing: implication of regional secondary formation, Atmos. Chem. Phys., 10, 947–959, doi:10.5194/acp-10-947-2010, 2010, 2010.

Hand, J. L. and Kreidenweis, S. M.: A New Method for Retrieving Particle Refractive Index and Effective Density from Aerosol Size Distribution Data, Aerosol Sci. Tech., 36, 1012-1026, doi:10.1080/02786820290092276, 2002.

Hatch, L. E., Pratt, K. A., Huffman, J. A., Jimenez, J. L., and Prather, K. A.: Impacts of Aerosol Aging on Laser Desorption/Ionization in Single-Particle Mass Spectrometers, Aerosol Sci. Tech., 48, 1050-1058, doi:10.1080/02786826.2014.955907, 2014.

Healy, R. M., Sciare, J., Poulain, L., Crippa, M., Wiedensohler, A., Prévôt, A. S. H., Baltensperger, U., Sarda-Estève, R., McGuire, M. L., Jeong, C. H., McGillicuddy, E., O'Connor, I. P., Sodeau, J. R., Evans, G. J., and Wenger, J. C.: Quantitative determination of carbonaceous particle mixing state in Paris using single-particle mass spectrometer and aerosol mass spectrometer measurements, Atmos. Chem. Phys., 13, 9479-9496, doi:10.5194/acp-13-9479-2013, 2013.

Jimenez, J. L.: New particle formation from photooxidation of diiodomethane (CH2I2), J. Geophys. Res., 108, doi:10.1029/2002jd002452, 2003.

Knutson, E. O. and Whitby, K. T.: Aerosol classification by electric mobility: Apparatus, theory, and applications, J. Aerosol Sci., 6, 443-451, doi:10.1016/0021-8502(75)90060-9, 1976.

Li, K., Ye, X., Pang, H., Lu, X., Chen, H., Wang, X., Yang, X., Chen, J., and Chen, Y.: Temporal variations in the hygroscopicity and mixing state of black carbon aerosols in a polluted megacity area, Atmos. Chem. Phys., 18, 15201-15218, doi:10.5194/acp-18-15201-2018, 2018.

Li, L., Li, M., Huang, Z., Gao, W., Nian, H., Fu, Z., Gao, J., Chai, F., and Zhou, Z.: Ambient particle characterization by single particle aerosol mass spectrometry in an urban area of Beijing, Atmos. Environ., 94, 323-331, doi:10.1016/j.atmosenv.2014.03.048, 2014.

Li, L., Huang, Z., Dong, J., Li, M., Gao, W., Nian, H., Fu, Z., Zhang, G., Bi, X., Cheng, P., and Zhou, Z.: Real time bipolar time-of-flight mass spectrometer for analyzing single aerosol particles, Int. J. Mass Spectrom., 303, 118-124, doi:10.1016/j.ijms.2011.01.017, 2011.

Liu, D., Joshi, R., Wang, J., Yu, C., Allan, J. D., Coe, H., Flynn, M. J., Xie, C., Lee, J., Squires, F., Kotthaus, S., Grimmond, S., Ge, X., Sun, Y., and Fu, P.: Contrasting physical properties of black carbon in urban Beijing between winter and summer, Atmos. Chem. Phys., 19, 6749-6769, doi:10.5194/acp-19-6749-2019, 2019.

Lu, S., Tan, Z., Liu, P., Zhao, H., Liu, D., Yu, S., Cheng, P., Win, M. S., Hu, J., Tian, L., Wu, M., Yonemochi, S., and Wang, Q.: Single particle aerosol mass spectrometry of coal combustion particles associated with high lung cancer rates in Xuanwei and Fuyuan, China, Chemosphere, 186, 278-286, doi:10.1016/j.chemosphere.2017.07.161, 2017.

Moffet, R. C., de Foy, B., Molina, L. T., Molina, M. J., and Prather, K. A.: Measurement of ambient aerosols in northern Mexico City by single particle mass spectrometry, Atmos. Chem. Phys., 8, 4499–4516, doi:10.5194/acp-8-4499-2008, 2008.

Peng, L., Li, L., Zhang, G., Du, X., Wang, X., Peng, P. a., Sheng, G., and Bi, X.: Technical note: Measurement of chemically resolved volume equivalent diameter and effective density of particles by AAC-SPAMS, Atmos. Chem. Phys., 21, 5605-5613, doi:10.5194/acp-21-5605-2021, 2021.

Pratt, K. A., DeMott, P. J., French, J. R., Wang, Z., Westphal, D. L., Heymsfield, A. J., Twohy, C. H., Prenni, A. J., and Prather, K. A.: In situ detection of biological particles in cloud ice-crystals, Nat. Geosci., 2, 398-401, doi:10.1038/ngeo521, 2009.

Silva, P. J., Liu, D. Y., Noble, C. A., and Prather, K. A.: Size and Chemical Characterization of Individual Particles Resulting from Biomass Burning of Local Southern California Species, Environ. Sci. Technol., 33, 3068-3076, doi:10.1021/es980544p 1999.

Spencer, M. T., Shields, L. G., and Prather, K. A.: Simultaneous Measurement of the Effective Density and Chemical Composition of Ambient Aerosol Particles, Environ. Sci. Technol., 41, 1303-1309, doi:10.1021/es061425+ 2007.

Su, B., Zhang, G., Zhuo, Z., Xie, Q., Du, X., Fu, Y., Wu, S., Huang, F., Bi, X., Li, X., Li, L., and Zhou, Z.: Different characteristics of individual particles from light-duty diesel vehicle at the launching and idling state by AAC-SPAMS, J. Hazard. Mater., 418, 126304, doi:10.1016/j.jhazmat.2021.126304, 2021.

Sun, J., Li, Y., Xu, W., Zhou, W., Du, A., Li, L., Du, X., Huang, F., Li, Z., Zhang, Z., Wang, Z., and Sun, Y.: Single-particle volatility and implications for brown carbon absorption in Beijing, China, Sci. Total Environ., 854, 158874, doi:10.1016/j.scitotenv.2022.158874, 2022a.

Sun, J., Sun, Y., Xie, C., Xu, W., Chen, C., Wang, Z., Li, L., Du, X., Huang, F., Li, Y., Li, Z., Pan, X., Ma, N., Xu, W., Fu, P., and Wang, Z.: The chemical composition and mixing state of BC-containing particles and the implications on light absorption enhancement, Atmos. Chem. Phys., 22, 7619-7630, doi:10.5194/acp-22-7619-2022, 2022b.

Tavakoli, F. and Olfert, J. S.: An instrument for the classification of aerosols by particle relaxation time: theoretical models of the aerodynamic aerosol classifier, Aerosol Sci. Tech., 47, 916-926, doi:10.1080/02786826.2013.802761, 2013.

Toner, S. M., Sodeman, D. A., and Prather, K. A.: Single particle characterization of ultrafine and accumulation mode particles from heavy duty diesel vehicles using aerosol time-of-flight mass spectrometry, Environ. Sci. Technol., 40, 3912-3921, doi:10.1021/es051455x, 2006.

Toner, S. M., Shields, L. G., Sodeman, D. A., and Prather, K. A.: Using mass spectral source signatures to apportion exhaust particles from gasoline and diesel powered vehicles in a freeway study using UF-ATOFMS, Atmospheric Environment, 42, 568-581, doi:10.1016/j.atmosenv.2007.08.005, 2008.

Wang, H., An, J., Shen, L., Zhu, B., Xia, L., Duan, Q., and Zou, J.: Mixing state of ambient aerosols in Nanjing city by single particle mass spectrometry, Atmos. Environ., 132, 123-132, doi:10.1016/j.atmosenv.2016.02.032, 2016.

Xie, C., He, Y., Lei, L., Zhou, W., Liu, J., Wang, Q., Xu, W., Qiu, Y., Zhao, J., Sun, J., Li, L., Li, M., Zhou, Z., Fu, P., Wang, Z., and Sun, Y.: Contrasting mixing state of black carbon-containing particles in summer and winter in Beijing, Environ. Pollut., 263, 114455, doi:10.1016/j.envpol.2020.114455, 2020.

Zelenyuk, A., Imre, D., and Cuadra-Rodriguez, L. A.: Evaporation of Water from Particles in the Aerodynamic Lens Inlet: An Experimental Study, Anal. Chem., 78, 6942-6947, doi:10.1021/ac061184o, 2006.

Zhang, G., Bi, X., Lou, S., Li, L., Wang, H., Wang, X., Zhou, Z., Sheng, G., Fu, J., and Chen, C.: Source and mixing state of iron-containing particles in Shanghai by individual particle analysis, Chemosphere, 95, 9-16, doi:10.1016/j.chemosphere.2013.04.046, 2014.

Zhang, T., Claeys, M., Cachier, H., Dong, S., Wang, W., Maenhaut, W., and Liu, X.: Identification and estimation of the biomass burning contribution to Beijing aerosol using levoglucosan as a molecular marker, Atmos. Environ., 42, 7013-7021, doi:10.1016/j.atmosenv.2008.04.050, 2008.

Zhang, Y., Pei, C., Zhang, J., Cheng, C., Lian, X., Chen, M., Huang, B., Fu, Z., Zhou, Z., and Li, M.: Detection of polycyclic aromatic hydrocarbons using a high performance-single particle aerosol mass spectrometer, J. Environ. Sci., 124, 806-822, doi:10.1016/j.jes.2022.02.003, 2022.

Zhong, Q., Cheng, C., Li, M., Yang, S., Wang, Z., Yun, L., Liu, S., Mao, L., Fu, Z., and Zhou, Z.: Insights into the different mixing states and formation processes of amine-containing single particles in Guangzhou, China, Sci. Total. Environ., 846, 157440, doi:10.1016/j.scitotenv.2022.157440, 2022.

Zhu, S., Li, L., Wang, S., Li, M., Liu, Y., Lu, X., Chen, H., Wang, L., Chen, J., Zhou, Z., Yang, X., and Wang, X.: Development of an automatic linear calibration method for high-resolution single-particle mass spectrometry: improved chemical species identification for atmospheric aerosols, Atmos. Meas. Tech., 13, 4111-4121, doi:10.5194/amt-13-4111-2020, 2020.